Product-to-intermediate relay achieving complete oxygen reduction reaction (cORR) with Prussian blue integrated nanoporous polymer cathode in fuel cells

Tawatchai Kangkamano, Mikhail Vagin, Lingyin Meng, Panote Thavarungkul, Proespichaya Kanatharana, Xavier Crispin and Wing Cheung Mak

Kangkamano, T., Vagin, M., Meng, L., Thavarungkul, P., Kanatharana, P., Crispin, X., Mak, W. C., (2020), Product-to-intermediate relay achieving complete oxygen reduction reaction (cORR) with Prussian blue integrated nanoporous polymer cathode in fuel cells, *Nano Energy*, 78, 105125.
https://doi.org/10.1016/j.nanoen.2020.105125

Product-to-Intermediate Relay Achieving Complete Oxygen Reduction Reaction (cORR) with Prussian Blue Integrated Nanoporous Polymer Cathode in Fuel Cells

Tawatchai Kangkamano,[1,3,4,#,δ] Mikhail Vagin,[2,#,] Lingyin Meng,[1] Panote Thavarungkul,[3,5] Proespichaya Kanatharana,[3,4] Xavier Crispin,[2] and Wing C. Mak,[1,*]*

[1]Department of Physics, Chemistry and Biology (IFM), Linköping University, 58183 Linköping, Sweden

[2]Laboratory of Organic Electronics, Department of Science and Technology (ITN), Linköping University, 601 74, Norrköping, Sweden

[3]Center of Excellence for Trace Analysis and Biosensor, Faculty of Science, Prince of Songkla University, Hat Yai, Songkhla, 90112, Thailand

[4]Department of Chemistry, Faculty of Science, Prince of Songkla University, Hat Yai, Songkhla, 90112, Thailand

[5]Department of Physics, Faculty of Science, Prince of Songkla University, Hat Yai, Songkhla, 90112, Thailand

#These authors contributed equally.

δ Current address: Department of Chemistry, Faculty of Science, Thaksin University, Papayom, Phattalung, 93110, Thailand

*Correspondence: mikhail.vagin@liu.se; wing.cheung.mak@liu.se

KEYWORDS

Complete oxygen reduction reaction, poly(3,4-ethylenedioxythiophene), Prussian blue, cryosynthesis, proton-exchange membrane fuel cell.

ABSTRACT

The oxygen reduction reaction (ORR) is an essential process in electrocatalysis limiting the commercialization of sustainable energy conversion technologies, such as fuel cells. The use of conducting polymers as molecular porous and conducting catalysts obtained from the high abundance elements enables the route towards low cost and high-throughput fabrication of disposable plastic electrodes of fuel cells. Poly(3,4-ethylenedioxythiophene) (PEDOT) is a 2-electron ORR electrocatalyst yielding specifically hydrogen peroxide that limits the full utilization of chemical energy of oxygen. Here, we demonstrated an innovative product-to-intermediate relay approach achieving complete oxygen reduction reaction (cORR) with Prussian blue (PB) integrated microporous PEDOT cathode in fuel cells. The microporous structured PEDOT electrode prepared via a simple cryosynthesis allows the bulk integration and stabilization of the poor conducting PB co-catalyst into the PEDOT ion-electron conductor, while the microporous PEDOT allows effective oxygen diffusion into the matrix. We evaluated systematically the effect of sequential PEDOT 2-electron ORR followed by PB co-catalysis launching hydrogen peroxide reduction reaction (HPRR) into H_2O. This resulted in the establishment of electronic and ionic transport between PEDOT and PB catalyst enabling the combination of enhanced ORR electrocatalysis by means of the ORR course extension from 2- to 4-electron reduction to achieve cORR. The cORR performance delivered by the product-to-intermediate relay between microporous PEDOT and PB co-catalysis led to four times increase of power density of model proton-exchange membrane fuel cell (PEMFC) assembled from the polymer-based air-breathing cathode.

INTRODUCTION

The sluggish kinetics of the ORR limits the efficiency of oxygen-associated chemical-to-electrical energy interconversion technologies such as fuel cells and metal-air batteries. Cost-ineffective platinum group metals are commonly utilized as catalysts to speed up the ORR and to enhance the conversion performance[1, 2]. This motivates an intensive research on ORR catalysts based on non-critical raw materials and manufactured by low-cost processes.

The M–N–C (M = Fe, Ni, Co) system with N-coordinated transition metal structures as an active sites [3-10] is one of the most attractive among various platinum group metal-free ORR catalysts, because it may achieve comparable performance to that of platinum group metal catalysts by proper structure design[11]. Synthesized by pyrolysis, the M–N–C ORR catalysts reveal the ORR activity dependent on the structure of metal-, carbon- and nitrogen-containing precursors. Among the variety of precursors[8, 12-16], the pre-organized metal complexes have a benefit of high probability to maintain the active structure after the pyrolysis[17-19].

Among the M–N–C catalysts, PB is a cheap and well-known coordination compound with an ordered 3D framework structure that possesses a high density of iron II/III sites coordinated with nitrogen of cyanide groups [20], which is ideal for M-N-C ORR catalysts [11]. This inspired the use of PB and its analogs as pyrolysis precursors [21-25]. Surprisingly, there are still rare examples of PB and its analogs direct use as ORR catalysts due to the poor stability towards the desorption [26] and dissolution in alkaline media [27, 28]. The PB incorporation into the conducting polymer matrix is a strategy to achieve the operational stability [29], which was utilized in cathode of microbial fuel cell [30]. Conducting polymers are considered among the best mixed electron-ion conductors, which are crucial for all electrochemical technology. They are synthesized via low temperature processing of organic molecules and enable variety of upscaling strategies. Moreover, the electronic and ionic transport can be controlled by both morphology and composition [31, 32], which enables the possibilities of maximization of density of triple-phase boundaries and bulk integration of poor conductors. Poly(3,4-ethylenedioxythiophene) (PEDOT)

complexed with polystrenesulfonate (PSS) is one of the most widely used intrinsically conducting polymer due to water processability, high electrical conductivity (up to about 1,000 S/cm), and good air stability due to oxidative polymerization [33]. Importantly, PEDOT has an ORR activity [34, 35] via two electron process with a close to 100% yield of hydrogen peroxide [36].

To achieve a high efficiency of chemical-to-electrical energy conversion of gaseous reactants, it is necessary to optimize electronic, ionic and reactant (gas) transports and to integrate all of them in a unified gas diffusion electrode. Here we explored the use of cryosynthesis involving freezing and thawing steps [37-39] as a strategy to control the morphology and the composition in PB- PEDOT composite for high efficiency air-breathing cathode fabrication. The effects of PB integration on both semiconductor properties of conducting polymer and the efficiency of chemical-to-electrical energy conversion via ORR elecrocatalysis were systematically evaluated. The enhancement of ORR efficiency by the PB integration within PEDOT was observed during material characterization and fuel cell operation. It was mainly attributed due to the addition of hydrogen peroxide reduction reaction (HPRR) triggering product-to-intermediate relay towards the series (2+2) complete ORR (cORR) process (Fig. 1A).

EXPERIMENTAL METHODS

Materials. 3,4-ethylenedioxythiophene (EDOT), poly-(sodium 4-styrenesulfonate) (NaPSS; MW ~1,000,000 g/mol), iron (III) chloride ($FeCl_3$) and potassium ferricyanide ($K_3[Fe(CN)_6]$) were from Sigma-Aldrich (St. Louis, USA). Potassium chloride (KCl), potassium hydrogen phosphate (K_2HPO_4) and potassium dihydrogen phosphate (KH_2PO_4) were from Merck (Damstadt, Germany). All chemicals used were of analytical grade and used as received without any further purification. Phosphate buffer solution (PBS, 0.10 M containing 0.10 M KCl, pH 7.40) was freshly prepared in ultrapure water purified using a Millipore-Q system (Scientific Support, Inc., USA).

Electrode preparation. A glassy carbon electrode (GCE) in a configuration of rotating disk electrode (RDE) (Pine, USA) or rotating ring-disk electrode (RRDE) setups (Pine, USA) (5.0 mm diameter) were sequentially polished to a mirror-like surface with 1.0, 0.3 and 0.05 μm alumina

slurry and rinsed thoroughly with distilled water in each polishing step. To prepare the PEDOT:PSS-PB composite, 0.038 g of NaPSS (0.038 μmol) dissolved in 0.50 mL of deionized water was mixed with 160 μL of EDOT monomer (1.5 mmol) followed by a 10 min sonication to obtain a uniform milky dispersion. A 25 μL of the EDOT:PSS suspension was then combined with 2.5 μL of 4.4 M $FeCl_3$ (oxidizing agent) and 5.0 μL of PB, prepared in advance by mixing of 500 mM $FeCl_3$ and 500 mM $K_3[Fe(CN)_6]$ in 10 mM HCl solution. After a 5 min vigorously stirring, 1.5 μL aliquot was drop casted onto the electrode surface, stored at −20 ˚C for at least 24 h before thawing at 4 ˚C for 30 min to achieve the PEDOT:PSS-PB cryogel. The modified electrode was then dried at 60 ˚C for 1 hour in an oven. For comparison, PB-free PEDOT:PSS cryogel-modified electrodes were also prepared by the same procedure. Bulk-structured non-porous PEDOT:PSS-PB modified electrodes were prepared without freezing and thawing steps.

Surface morphologies of the cryogel-modified electrodes were observed using a scanning electron microscope (SEM, PHENOM PRO, FEI, Netherlands). Fourier Transform Infrared (FT-IR) spectra were from a VERTEX 70 (Bruker, USA) spectrophotometer.

Electrochemical measurement. Electrochemical measurement of the modified electrodes were performed in a batch cell equipped with a gas flow system Autolab type III bi-potentiostat (Metrohm Autolab, Netherlands). The electrolyte is 0.10 M PBS containing 0.10 M KCl (pH 7.40). Cyclic voltammetry measurements were carried out with a three-electrode system comprised a modified glassy carbon working electrode, a silver/silver chloride reference electrode and a platinum wire counter electrode. The hydrodynamic electrode measurements were done on rotating disk electrode and rotating ring disk electrode (Pine Research Instrumentation Inc.) at room temperature in oxygen- or argon-saturated electrolyte. The LSV results were subtracted by the background current recorded in an argon-saturated electrolyte.

In-situ resistometry was carried out on a two-terminal gold interdigitated microelectrode array on glass (15 μm gap; MicruX Technologies, Spain) using bi-potentiostat to control two independent working electrodes. The channel current was calculated by means of subtraction of

current recorded on first working electrode with 0 mV bias with respect to the second working electrode from the current recorded with 50 mV bias. The apparent film resistance was calculated as a quotient of 50 mV bias to channel current.

Fuel cell measurements. The PEMFC were elaborated from activated Nafion 115 membranes, Teflon gaskets and fuel cell body (FuelCellStore Inc.) with air-breathing cathode and constant flow of humidified hydrogen through anode. A 500 μL of the PEDOT:PSS-PB composite slurry was drop casted on a 3x3 cm^2 gas diffusion electrode (graphite paper AvCarb GDS2230, FuelCellStore Inc.), kept at −20 ˚C for at least 24 h, thawed at 4 ˚C for 30 min and dried at 60 ˚C for 1 h in an oven, respectively. Graphite cloth with high platinum load (0.3 mg/cm^2 PtC, 40 % on gas diffusion electrode; FuelCellStore Inc.) was utilized as a hydrogen anode. The membrane electrode assembly was elaborated by pressing (at 60 ◦C) with anode and cathode on activated Nafion 115 membrane using 100 μL of 5.0% Nafion solution (Sigma-Aldrich). The devices were evaluated at room temperature by steady-state polarization using decade resistor box (Swema, Sweden) and multimeter (Keithley, Tektronix, Germany).

RESULTS AND DISCUSSION

The simplified landscape of experimental ORR pathways [40] includes two alternative trails: 4-electron (‘direct’) pathway, where water is formed without any detectable intermediates, and 2-electron (‘series’) pathway, where the hydrogen peroxide is formed as an intermediate [41]. The mechanism of ORR on pure PEDOT can be rationalized as series pathway [36, 42], where two-electronic reduction precede O-O bond breaking yielding the hydrogen peroxide as a major product. Being advantageous for a certain applications [36], series pathway of ORR with a hydrogen peroxide production is objectionable in chemical-to-electrical energy conversion technologies, because, firstly, the resource of oxygen as an oxidizer is not fully utilized, and, secondly, the hydrogen peroxide management complicates the device operation due to the possible destabilization [43-45]. The transition metal ions impurities can change the ORR pathway [46,

47]. We utilized this effect here for elongation of electrocatalysis pathway from 2-electron to series 4-electron to accomplish cORR to water by addition of PB as a co-catalyst of hydrogen peroxide reduction reaction (HPRR) [48, 49]. PB can be considered as a true 2-electron HPRR catalyst within ca. 0.30 V window of applied cathodic polarization preceding ORR [26]. This allowed us the systematic evaluation of the effect of product-to-intermediate relay on cORR electrocatalysis efficiency. The porosity of catalyst composite achieved by aqueous cryosynthesis, an environmentally-friendly one-step protocol, allowed the functional evaluation of composite-based hydrogen PEMFC. To achieve the porosity of polymer-based catalysts for effective gaseous reactant/product mass transport in the course of the PEMFC operation we utilized aqueous cryosynthesis of PEDOT:PSS-based composites followed by thawing [50] on graphite gas diffusion electrode, which, as we believe, possess a technological relevance. The cryosynthesis yielded the microscale phase-segregated frozen composite available for subsequent water phase removal during thawing. The structured films showed a honey comp-like porous structure (Fig. 1B, S1) with an average pore diameter of 0.43±0.23 μm. We further compared the morphologies of PEDOT:PSS-PB prepared by bulk synthesis (Fig. S1A) and cryosynthesis (Fig. S1B). SEM images show the cryosynthesis leading to the formation of porous microstructured film, while the control bulk synthesis resulted in a non-porous compacted bulk film.

Firstly, we confirmed the integration of co-catalyst into the conducting polymer matrix by physio-chemical methods. The presence of the small absorption band on composite FTIR spectrum (2067 cm^{-1}) assigned to CN stretching vibration in Fe^{II}–CN–Fe^{III} of PB [51, 52] in combination with a typical set of bands for PEDOT [53, 54] and sulfonic acid group of PEDOT:PSS (Fig. 1C, Supporting Note 1) confirmed the integration of PB into PEDOT:PSS matrix. X-ray photoelectron spectroscopy (XPS) was performed to investigate the chemical characteristics of the PEDOT:PSS/PB composites. The full survey spectrum in Figure 1D showed the sharp bands of S2p, C1s and O1s at 165.6, 284.8 and 531.8 eV respectively, which are ascribed to the PEDOT and PSS moieties. Except these, the two bands at about 396.5 and 707.5 eV are assigned to N1s

and Fe2p, indicating the existence of C≡N and Fe element originating from Prussian blue ($Fe_4[Fe(CN)_6]^3$). The voltammetry on composite-modified electrodes (Fig. 2A) revealed the overlay between the box-shaped capacitive region of conducting polymer and sharp redox peaks corresponding to PB/Prussian white faradaic phenomena. The increase of the inorganic material content represented by the increase of redox peak currents led the extension of the conductivity window of polymer. The cathodic limit (e.g. -1.2 V) of applied potentials is featured with small values of recorded currents due to the achievement of de-doped insulator state of conducting polymer. On the contrast, large currents assigned to the electrocapacitive phenomena within the doped highly conductive state of the polymer are observed at the anodic limit (e.g. 0.50 V) [55]. Importantly, the capacitive currents observed for the PB-doped PEDOT:PSS composite electrode are almost equal for various PB content, which illustrate the maintenance of the same amount of conducting polymer in the composite and allows the systematic evaluation of the role of PB. The presence of PB in the composite led to the cathodic shift of the potential threshold for the doping/de-doping transition of PEDOT (Inset of Fig. 2A; ca. -0.80 V for 500 mM, -0.60 V of 300 mM and -0.50 V for 100 mM of PB), which is a feature of the redox doping of conducing polymer [56].

To quantify the effect PB on the redox doping threshold potential of the polymer, we utilized in-situ resistometry on microelectrochemical electrode setup [57, 58] (Fig. 2B). The clear transition between highly conductive state of polymer characterized with low film resistance (0.70 V – 0 V) and partial de-doped state of higher resistance (0 V – -0.80 V) is observed for both blank and PB-doped PEDOT. The integration of PB led to the additional kinetic effect on polymer conductivity visible as a film resistance decrease in both highly-doped and partial de-doped states of polymer (20% and 80% at 0.50 V and -0.40 V, respectively). The significant kinetic effect on doping/de-doping behavior of films is seen at the high scan rate (see Fig. S2) characterized with an ionic transport control as a rate determining step of an electrode process. The presence of the inorganic redox material yielded the significant decrease in film resistance in comparison with

blank conducting polymer. This effect illustrates the kinetic decoupling of the slow redox conversion of PB from the fast PEDOT de-doping due to the ion trapping within the inorganic material [59].

The cORR electrocatalysis has been investigated by the steady-state voltammetry on film-modified hydrodynamic electrode setup (Fig. 3A). The ohmic drop-compensated steady-state voltammetry showed both higher faradaic currents (e.g. more than 60% increase at 0.25 V) and lower overpotential of PB-PEDOT composite electrode compared to both the glassy carbon and the PEDOT:PSS electrode. The appearance of hydrogen peroxide electrocatalysis for both oxidation and reduction reactions is manifested by the increase of steady-state currents in both negative (0.3 V – -0.6 V) and positive (0.5 V – 0.6 V) directions, respectively, observed in oxygen-free environment in the presence of hydrogen peroxide. The increase of reduction rate also enables the achievement of the limitation by the hydrogen peroxide diffusion (Figure S3, lower than 0 V). Thus, the observed increase of ORR electrocatalytic currents illustrates the contribution from additional HPRR process accomplishing a series 4-electron reduction on PB-doped PEDOT. Below 0.1 V, PB can contribute also with its inherent 4-electron ORR [26].

Conducting polymers are recognized as mixed electron-ion conductors [60, 61]. Indeed, the modulation of electronic charge within the polymer film imposed by the change of applied potential is ensured with the counter-ion transport for the film electroneutrality maintenance. This assigns a distinctive role of PEDOT as advanced matrix for inorganic electrocatalyst immobilization. Firstly, it enables the electronic access to the inorganic insulator by bulk integration. Secondly, it maintains ionic transport essential for the PB redox process stability and for the neutralization of the final product (hydroxide). The microstructuring facilitates the ionic transport, which leads to the slight increase of redox material accessibility (Fig. S4). Thirdly, it contributes with intrinsic 2-electron electrocatalysis yielding convertible product. Fourthly, the polymer prevents PB desorption from hydrodynamic electrode.

Importantly, the increase of PB content in the catalytic composite led to the increase of the total ORR currents (see Fig. S5), which shows that HPRR is a rate determining step in a whole series 4-electron ORR. The modulation of the rotation speed allowed the observation of Tafel regions for ORR on the investigated electrocatalysts (see Fig. S6). The change of rate determining step of a whole ORR with the integration of inorganic co-catalyst has been confirmed with a stabi slope change observed for PB-doping of catalyst (from 140 mV dec^{-1} on PEDOT:PSS to 80 mV dec^{-1} on PB-doped PEDOT:PSS), which is approaching to the slope for commercial platinum-on-carbon catalyst (~ 66 mV dec^{-1}) [62]. Being relevant for the PEMFC operational conditions, the acidic electrolyte showed the change of rate determining step of cORR electrocatalysis on PEDOT:PSS-PB composite manifested with a higher Tafel slope up to 170 mV dec^{-1}.

The half-wave potential calculated from the steady-state voltammetry data (Fig. 3A) and estimated maximum kinetic current (Fig. S6) of ORR on PB-PEDOT:PSS composite electrode were 0.33 V (vs RHE) and 0.5 mA cm^{-2}, respectively, which is humble in comparison with the characteristics of state of the art platinum group metal-free ORR electrocatalysts [9, 10].

The mechanistic evaluation of developed cORR catalysts was carried out on rotating ring disk electrode setup (Supporting Note 2). The presence of inorganic HPRR catalyst in the polymer composite led to the significant decrease of yield of hydrogen peroxide in comparison with blank and PEDOT:PSS-modified rotating disk electrode (Fig. 3B, S8). This confirms the launching of HPRR co-catalysis in a whole cORR electrocatalysis phenomenon visible as decrease of the quantified amount of intermediate peroxide (e.g. peroxide yields of 3.2 %, 13 % and 21% for PB-doped PEDOT:PSS, glassy carbon and PEDOT:PSS at -0.50 V). Coherently, the Koutecky-Levich analysis of recorded disk electrode currents on thin films of catalytic composite [63] showed larger numbers of electrons transferred per oxygen molecule (Fig. 3C) from PB-doped PEDOT:PSS electrode compared to the pristine PEDOT:PSS. The number of electrons transferred is close to 4 electrons with PB-doped PEDOT:PSS at some potential. Being relevant for PEMFC, the evaluation of cORR electrocatalysts in acidic environment yielded the conformed larger number

of transferred electrons per reactant molecule on PB-doped polymer composite (see Fig. S9). The kinetic analysis in the frame of Damjanovic approach [64, 65] showed up to one order increase of HPRR rate constant in the course of ORR in the presence of PB (Supporting Note 3) compared to the pristine PEDOT:PSS. The obtained quantification data of electrocatalysis in combination with larger total currents recorded on PB-doped polymer-based composite systematically illustrate the impact of the additional 2-electron co-catalysis of HPRR on the efficiency of whole cORR electrocatalysis maximizing the generated power output [44].

To appraise the HPRR co-catalysis impact on the efficiency of chemical-to-electrical energy conversion, we performed a comparative evaluation of polymer-based air-breathing cathodes in hydrogen PEMFC (Fig. 4). The polarization curves obtained on cathode-limited PEMFC in a presence of PB (3.7 mg cm^{-2}) on air-breathing gas diffusion electrode showed both significantly smaller activation loss and larger open circuit potential in comparison with the device based on blank PEDOT:PSS, which resulted in a significantly larger value of maximum power density. Although the design of the fuel cell was not optimized, we varied one parameter, i.e the type of material at the air cathode of the hydrogen fuel cell. The PB-doped PEDOT:PSS electrode appears as true platinum group metal-free catalytic composite because of the an additional HPRR co-catalysis of PB compared to PEDOT:PSS. As soon as HPRR is a rate-determining step in in a whole 2+2 ORR, we utilized the composite of maximized PB content for air cathode modification. The presence of PB showed a minor change of porosity in comparison with blank PEDOT:PSS (Tab. S1) defining the negligible effect of the mass transport variation in polymer cathodes by the inorganic co-catalyst integration. As a result, the PEM fuel cell, with approximately the same open circuit voltage of 0.50 V deliver 0.018 mW cm^{-2} of the maximum power density at 0.18 V (0.10 mA cm^{-2}), which is almost 4 times higher than obtained with the device based on the 2-electron ORR PEDOT:PSS cathode.

CONCLUSIONS

To conclude, we successfully integrate PB as inorganic HPRR catalyst into the conducting polymer PEDOT:PSS matrix via the aqueous cryosynthesis. The PB-doped PEDOT:PSS nanocomposite is evaluated by physical-chemical methods and support the stabilization of PB, which elongates the ORR pathway from 2- to a series of 4-electronic reduction to achieve cORR process as revealed by hydrodynamic voltammetry. In the nanocomposite, the PEDOT:PSS matrix reduces oxygen to hydrogen peroxide, while the PB doping acts as co-catalysis via HPRR as a product-to-intermediate relay. PEDOT:PSS is thus an advanced matrix to immobilize an inorganic co-catalyst in its bulk because the conducting polymer is a good mixed ionic-electronic conductor, thus bringing both electrons and ions in close vicinity of the PB particles stored within the bulk of the nanocomposite electrode. The addition of PB-associated redox process into the electrocapacitive phenomena of polymer led to the changes of charge storage kinetics of composite semiconductor. The cORR performance enhancement by inorganic co-catalyst was demonstrated with the construction of an effective plastic air-breathing gas diffusion electrode in a hydrogen PEMFC: one of the first half polymer-based fuel cells.

FIGURES

Figure 1. PB-doped PEDOT:PSS air breathing cathode. (A) The enhancement of cORR efficiency by the PB-doped PEDOT:PSS resulted from the addition of hydrogen peroxide reduction reaction (HPRR) triggering product-to-intermediate relay towards the series (2+2) cORR; (B) SEM images of the microporous PB-doped PEDOT:PSS (lower insert shows the PB-doped PEDOT:PSS air breathing cathode); (C) FTIR spectrum and (D) XPS spectrum of the PEDOT:PSS/PB composite.

Figure 2. Integration of PB into PEDOT:PSS. (A) Cyclic voltammograms recorded on glassy carbon modified with PEDOT:PSS cryogel film fabricated from different PB concentrations (100, 300 and 500 mM as black, red and blue curves, respectively; scan rate 100 mV s^{-1}); (B) in-situ

resistometry on blank and PB-modified PEDOT:PSS (scan rate 5.0 mV s^{-1}, 0.10 M PBS (pH 7.40), 0.10 M KCl).

Figure 3. The elongation of electrocatalysis pathway from 2- to 4-electron ORR. (A) Ohmic drop-corrected steady-state polarization curves obtained in oxygen- and argon-saturated electrolyte (filled and open symbols, respectively; 0.10 M PBS (pH 7.4), 0.10 M KCl) on blank, PEDOT:PSS- and PEDOT:PSS-PB film-modified glassy carbon rotating disk electrode (black, red and blue symbols, respectively; magenta – in the presence of hydrogen peroxide (3.0 mM; argon-saturated electrolyte; 2500 rpm)); (B) and (C) – potential dependencies of peroxide yield and the number of electrons transferred per oxygen molecules estimated for ORR on blank, PEDOT:PSS- and PEDOT:PSS-PB film-modified glassy carbon rotating disk electrode (black, red and blue symbols, respectively).

Figure 4. The effect of HPRR co-catalysis on the efficiency of hydrogen PEMFC. A: Sketch of polymer cathode PEMFC; B: The polarization curves and power density plots of cathode-limited PEMFC with blank and PB-doped PEDOT:PSS-based air-breathing cathode (red and blue symbols, respectively; 3.7 mg cm^{-2} of PB). Inset: photo of hydrogen PEMFC.

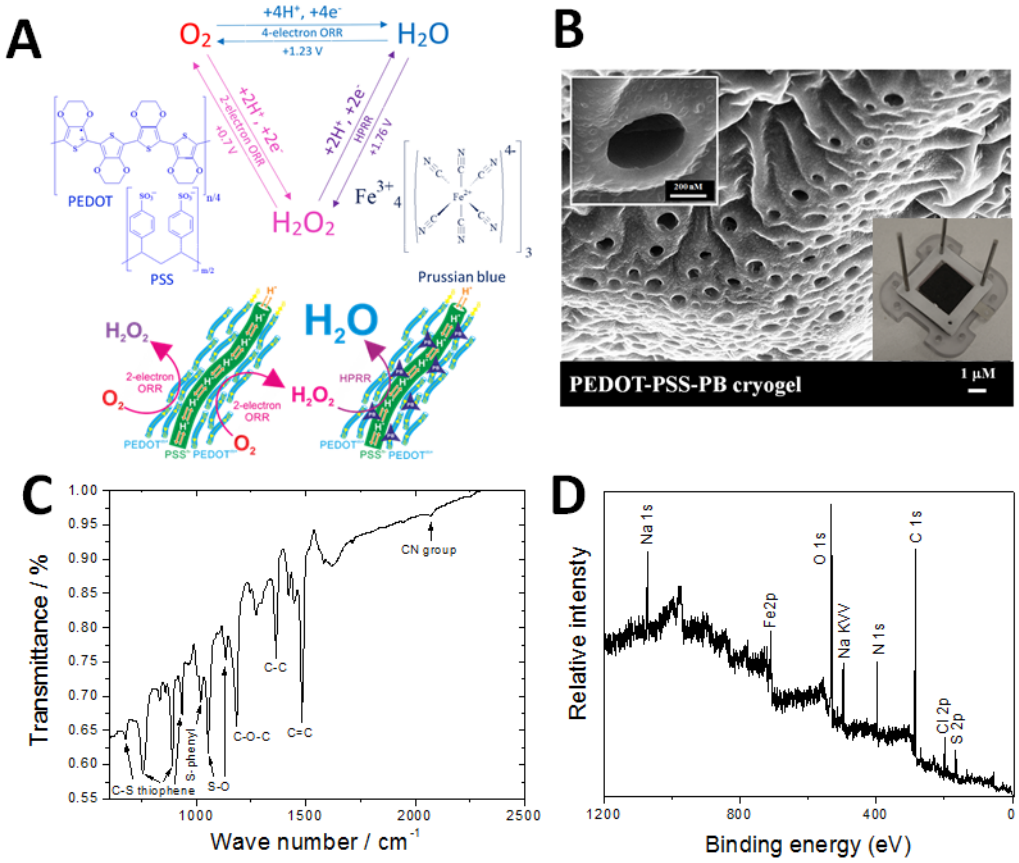
A
O2
+4H+, +4e-
4-electron ORR
+1.23 V
H2O
+2H+ +2e-
2-electron ORR
+0.7 V
H2O2
+2H+ +2e-
HPRR
+1.76 V
PEDOT
PSS
Fe3+4
Prussian blue
B
200 nM
PEDOT-PSS-PB cryogel
1 μM
C
Transmittance / %
Wave number / cm-1
CN group
C-C
C-O-C
C=C
S-phenyl
S-O
C-S thiophene
D
Relative intensty
Binding energy (eV)
Na 1s
Fe2p
O 1s
Na KVV
N 1s
C 1s
Cl 2p
S 2p

Figure 1.

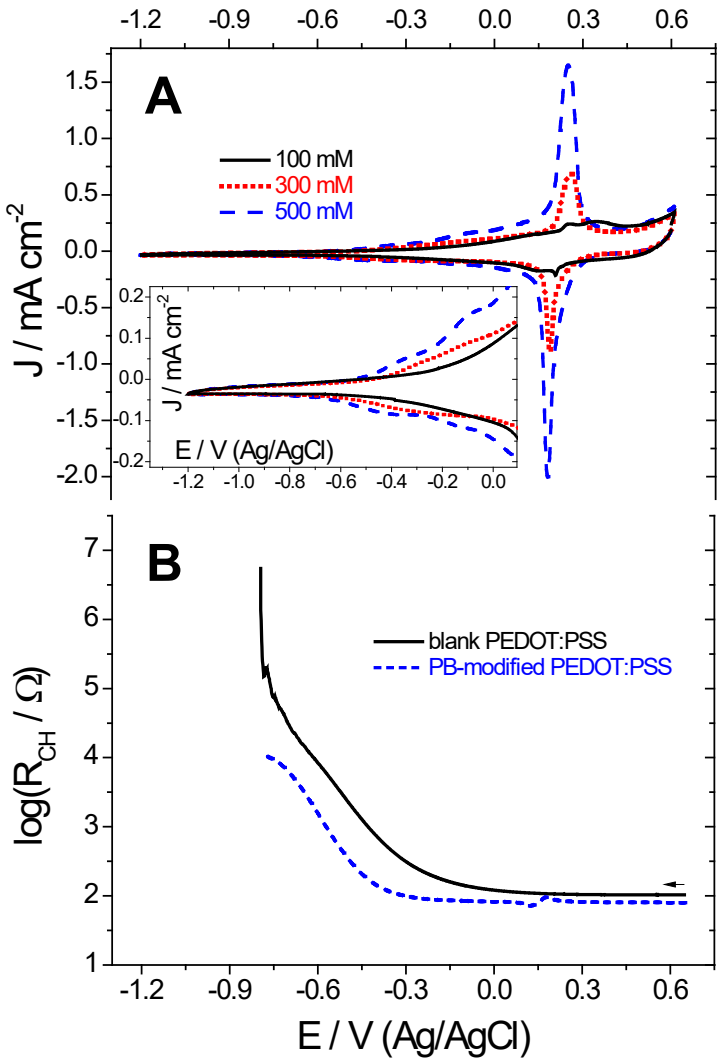
A
100 mM
300 mM
500 mM
J / mA cm-2
E / V (Ag/AgCl)
B
blank PEDOT:PSS
PB-modified PEDOT:PSS
log(RCH / Ω)
E / V (Ag/AgCl)

Figure 2.

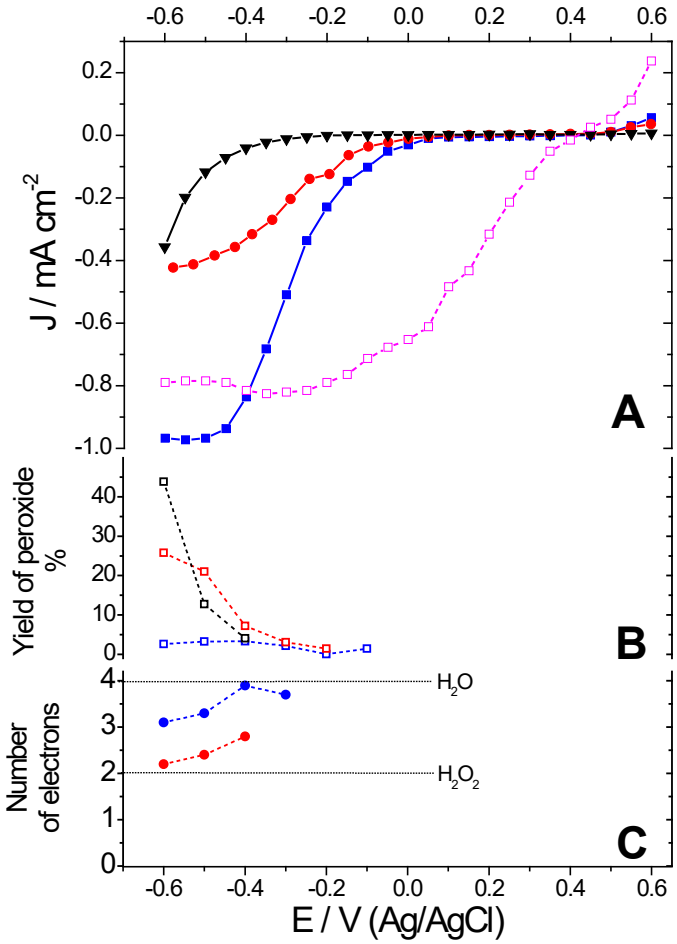
J / mA cm-2
A
Yield of peroxide %
B
Number of electrons
H2O
H2O2
C
E / V (Ag/AgCl)

Figure 3.

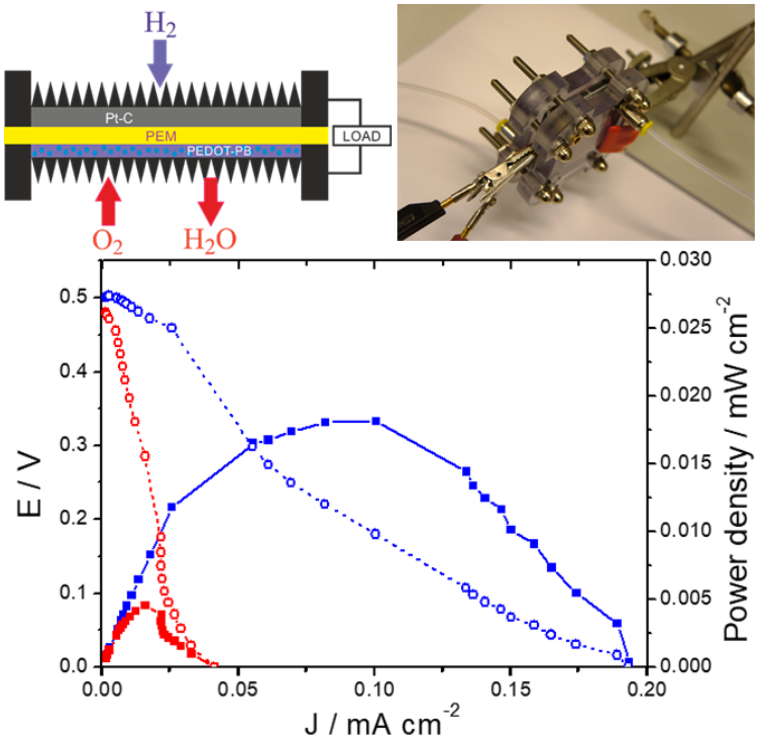
H2
Pt-C
PEM
PEDOT-PB
LOAD
O2
H2O
E / V
J / mA cm-2
Power density / mW cm-2
0.0
0.1
0.2
0.3
0.4
0.5
0.00
0.05
0.10
0.15
0.20
0.000
0.005
0.010
0.015
0.020
0.025
0.030

Figure 4.

Author Contributions

Conceptualization, M.Y.V., W.C.M. and T.K.; Methodology, M.Y.V., W.C.M. and T.K.; Investigation, M.Y.V., W.C.M., T.K., X.C. and L.M.; Writing – Original Draft, M.Y.V., W.C.M., P.T., P.K. and T.K.; Writing – Review & Editing, M.Y.V., W.C.M. and X.C.; Funding Acquisition, M.Y.V., W.C.M., P.T., P.K., X.C. and T.K.; Resources, M.Y.V. and W.C.M.; Supervision, M.Y.V., W.C.M., P.T. and P.K.

Notes

The authors declare no competing financial interest.

ACKNOWLEDGMENTS

The authors would like to acknowledge the National Science and Technology Development Agency (NSTDA), the Ministry of Science and Technology of Thailand, the Swedish Research Council (VR 2019-05577, Flexible metal-air primary batteries), the Swedish Government Strategic Research Area in Materials Science on Functional Materials at Linköping University (Faculty Grant SFO Mat LiU No. 2009 00971), and the Swedish Research Council (VR 2015-04434, paper fuel cells) for generous financial support to carry out this research.

REFERENCES

[1] M.H. Shao, Q.W. Chang, J.P. Dodelet, R. Chenitz, Recent Advances in Electrocatalysts for Oxygen Reduction Reaction, Chemical Reviews, 116 (2016) 3594-3657.

[2] C. Wang, N.M. Markovic, V.R. Stamenkovic, Advanced Platinum Alloy Electrocatalysts for the Oxygen Reduction Reaction, Acs Catalysis, 2 (2012) 891-898.

[3] J.K. Dombrovskis, H.Y. Jeong, K. Fossum, O. Terasaki, A.E.C. Palmqvist, Transition Metal Ion-Chelating Ordered Mesoporous Carbons as Noble Metal-Free Fuel Cell Catalysts, Chemistry of Materials, 25 (2013) 856-861.

[4] M. Ferrandon, A.J. Kropf, D.J. Myers, K. Artyushkova, U. Kramm, P. Bogdanoff, G. Wu, C.M. Johnston, P. Zelenay, Multitechnique Characterization of a Polyaniline-Iron-Carbon Oxygen Reduction Catalyst, Journal of Physical Chemistry C, 116 (2012) 16001-16013.

[5] F. Jaouen, J. Herranz, M. Lefevre, J.P. Dodelet, U.I. Kramm, I. Herrmann, P. Bogdanoff, J. Maruyama, T. Nagaoka, A. Garsuch, J.R. Dahn, T. Olson, S. Pylypenko, P. Atanassov, E.A. Ustinov, Cross-Laboratory Experimental Study of Non-Noble-Metal Electrocatalysts for the Oxygen Reduction Reaction, Acs Applied Materials & Interfaces, 1 (2009) 1623-1639.

[6] S. Kattel, P. Atanassov, B. Kiefer, Catalytic activity of Co-N-x/C electrocatalysts for oxygen reduction reaction: a density functional theory study, Physical Chemistry Chemical Physics, 15 (2013) 148-153.

[7] U.I. Kramm, M. Lefevre, N. Larouche, D. Schmeisser, J.P. Dodelet, Correlations between Mass Activity and Physicochemical Properties of Fe/N/C Catalysts for the ORR in PEM Fuel Cell via Fe-57 Mossbauer Spectroscopy and Other Techniques, Journal of the American Chemical Society, 136 (2014) 978-985.

[8] S.Q. Ma, G.A. Goenaga, A.V. Call, D.J. Liu, Cobalt Imidazolate Framework as Precursor for Oxygen Reduction Reaction Electrocatalysts, Chemistry-a European Journal, 17 (2011) 2063-2067.

[9] Z.K. Yang, Y. Wang, M.Z. Zhu, Z.J. Li, W.X. Chen, W.C. Wei, T.W. Yuan, Y.T. Qu, Q. Xu, C.M. Zhao, X. Wang, P. Li, Y.F. Li, Y. Wu, Y.D. Li, Boosting Oxygen Reduction Catalysis with Fe-N-4 Sites Decorated Porous Carbons toward Fuel Cells, Acs Catalysis, 9 (2019) 2158-2163.

[10] P.Q. Yin, T. Yao, Y. Wu, L.R. Zheng, Y. Lin, W. Liu, H.X. Ju, J.F. Zhu, X. Hong, Z.X. Deng, G. Zhou, S.Q. Wei, Y.D. Li, Single Cobalt Atoms with Precise N-Coordination as Superior Oxygen Reduction Reaction Catalysts, Angewandte Chemie-International Edition, 55 (2016) 10800-10805.

[11] X.J. Wang, L.R. Zou, H. Fu, Y.F. Xiong, Z.X. Tao, J. Zheng, X.G. Li, Noble Metal-Free Oxygen Reduction Reaction Catalysts Derived from Prussian Blue Nanocrystals Dispersed in Polyaniline, Acs Applied Materials & Interfaces, 8 (2016) 8436-8444.

[12] D. Zhao, J.L. Shui, C. Chen, X.Q. Chen, B.M. Reprogle, D.P. Wang, D.J. Liu, Iron imidazolate framework as precursor for electrocatalysts in polymer electrolyte membrane fuel cells, Chemical Science, 3 (2012) 3200-3205.

[13] G. Wu, K.L. More, C.M. Johnston, P. Zelenay, High-Performance Electrocatalysts for Oxygen Reduction Derived from Polyaniline, Iron, and Cobalt, Science, 332 (2011) 443-447.

[14] R. Silva, D. Voiry, M. Chhowalla, T. Asefa, Efficient Metal-Free Electrocatalysts for Oxygen Reduction: Polyaniline-Derived N- and O-Doped Mesoporous Carbons, Journal of the American Chemical Society, 135 (2013) 7823-7826.

[15] J. Herranz, F. Jaouen, M. Lefevre, U.I. Kramm, E. Proietti, J.P. Dodelet, P. Bogdanoff, S. Fiechter, I. Abs-Wurmbach, P. Bertrand, T.M. Arruda, S. Mukerjee, Unveiling N-Protonation and Anion-Binding Effects on Fe/N/C Catalysts for O-2 Reduction in Proton-Exchange-Membrane Fuel Cells, Journal of Physical Chemistry C, 115 (2011) 16087-16097.

[16] M. Bron, J. Radnik, M. Fieber-Erdmann, P. Bogdanoff, S. Fiechter, EXAFS, XPS and electrochemical studies on oxygen reduction catalysts obtained by heat treatment of iron phenanthroline complexes supported on high surface area carbon black, Journal of Electroanalytical Chemistry, 535 (2002) 113-119.

[17] S.W. Yuan, J.L. Shui, L. Grabstanowicz, C. Chen, S. Commet, B. Reprogle, T. Xu, L.P. Yu, D.J. Liu, A Highly Active and Support-Free Oxygen Reduction Catalyst Prepared from Ultrahigh-Surface-Area Porous Polyporphyrin, Angewandte Chemie-International Edition, 52 (2013) 8349-8353.

[18] E. Proietti, F. Jaouen, M. Lefevre, N. Larouche, J. Tian, J. Herranz, J.P. Dodelet, Iron-based cathode catalyst with enhanced power density in polymer electrolyte membrane fuel cells, Nature Communications, 2 (2011).

[19] R.L. Liu, C. von Malotki, L. Arnold, N. Koshino, H. Higashimura, M. Baumgarten, K. Mullen, Triangular Trinuclear Metal-N-4 Complexes with High Electrocatalytic Activity for Oxygen Reduction, Journal of the American Chemical Society, 133 (2011) 10372-10375.

[20] S. Juszczyk, C. Johansson, M. Hanson, A. Ratuszna, G. Malecki, Ferromagnetism of the Me3FE(CN)6 2-center -dot--H2O compounds, where Me = NI and CO, Journal of Physics-Condensed Matter, 6 (1994) 5697-5706.

[21] R.F. Zhou, S.Z. Qiao, An Fe/N co-doped graphitic carbon bulb for high-performance oxygen reduction reaction, Chemical Communications, 51 (2015) 7516-7519.

[22] L. Xu, G.Q. Zhang, J. Chen, Y.F. Zhou, G.E. Yuan, F.L. Yang, Spontaneous redox synthesis of Prussian blue/graphene nanocomposite as a non-precious metal catalyst for efficient four-electron oxygen reduction in acidic medium, Journal of Power Sources, 240 (2013) 101-108.

[23] J.B. Xi, Y.T. Xia, Y.Y. Xu, J.W. Xiao, S. Wang, (Fe,Co)@nitrogen-doped graphitic carbon nanocubes derived from polydopamine-encapsulated metal-organic frameworks as a highly stable and selective non-precious oxygen reduction electrocatalyst, Chemical Communications, 51 (2015) 10479-10482.

[24] J. Sanetuntikul, S. Shanmugam, Prussian Blue-Carbon Hybrid as a Non-Precious Electrocatalyst for the Oxygen Reduction Reaction in Alkaline Medium, Electrochimica Acta, 119 (2014) 92-98.

[25] D.H. Deng, L. Yu, X.Q. Chen, G.X. Wang, L. Jin, X.L. Pan, J. Deng, G.Q. Sun, X.H. Bao, Iron Encapsulated within Pod-like Carbon Nanotubes for Oxygen Reduction Reaction, Angewandte Chemie-International Edition, 52 (2013) 371-375.

[26] K. Itaya, N. Shoji, I. Uchida, Catalysis of the reduction of molecular-oxygene to water at prussian blue modified electrodes, Journal of the American Chemical Society, 106 (1984) 3423-3429.

[27] Z.W. Wang, H.K. Yang, B.W. Gao, Y. Tong, X.J. Zhang, L. Su, Stability improvement of Prussian blue in nonacidic solutions via an electrochemical post-treatment method and the shape evolution of Prussian blue from nanospheres to nanocubes, Analyst, 139 (2014) 1127-1133.

[28] S.G. Wu, J.P. Liu, X. Bai, W.G. Tan, Stability Improvement of Prussian Blue by a Protective Cellulose Acetate Membrane for Hydrogen Peroxide Sensing in Neutral Media, Electroanalysis, 22 (2010) 1906-1910.

[29] Y.J. Zou, L.X. Sun, F. Xu, Prussian Blue electrodepo sited on MWNTs-PANI hybrid composites for H2O2 detection, Talanta, 72 (2007) 437-442.

[30] L. Fu, S.J. You, G.Q. Zhang, F.L. Yang, X.H. Fang, Z. Gong, PB/PANI-modified electrode used as a novel oxygen reduction cathode in microbial fuel cell, Biosensors & Bioelectronics, 26 (2011) 1975-1979.

[31] K. Tybrandt, I.V. Zozoulenko, M. Berggren, Chemical potential-electric double layer coupling in conjugated polymer-polyelectrolyte blends, Science Advances, 3 (2017).

[32] A. Malti, J. Edberg, H. Granberg, Z.U. Khan, J.W. Andreasen, X.J. Liu, D. Zhao, H. Zhang, Y.L. Yao, J.W. Brill, I. Engquist, M. Fahlman, L. Wagberg, X. Crispin, M. Berggren, An Organic Mixed Ion-Electron Conductor for Power Electronics, Advanced Science, 3 (2016).

[33] B.L. Groenendaal, F. Jonas, D. Freitag, H. Pielartzik, J.R. Reynolds, Poly(3,4-ethylenedioxythiophene) and its derivatives: Past, present, and future, Advanced Materials, 12 (2000) 481-494.

[34] V. Gueskine, A. Singh, M. Vagin, X. Crispin, I. Zozoulenko, Molecular Oxygen Activation at a Conducting Polymer: Electrochemical Oxygen Reduction Reaction at PEDOT Revisited, a Theoretical Study, The Journal of Physical Chemistry C, accepted (2020).

[35] B. Winther-Jensen, O. Winther-Jensen, M. Forsyth, D.R. MacFarlane, High rates of oxygen reduction over a vapor phase-polymerized PEDOT electrode, Science, 321 (2008) 671-674.

[36] E. Mitraka, M. Gryszel, M. Vagin, M.J. Jafar, A. Singh, M. Warczak, M. Mitrakas, M. Berggren, T. Ederth, I. Zozoulenko, X. Crispin, E.D. Głowacki, Electrocatalytic Production of Hydrogen Peroxide with Poly(3,4-ethylenedioxythiophene) Electrodes, Advanced Sustainable Systems, 3 (2019) 1800110.

[37] A. Fatoni, A. Numnuam, P. Kanatharana, W. Limbut, C. Thammakhet, P. Thavarungkul, A highly stable oxygen-independent glucose biosensor based on a chitosan-albumin cryogel incorporated with carbon nanotubes and ferrocene, Sensors and Actuators B-Chemical, 185 (2013) 725-734.

[38] T. Kangkamano, A. Numnuam, W. Limbut, P. Kanatharana, P. Thavarungkul, Chitosan cryogel with embedded gold nanoparticles decorated multiwalled carbon nanotubes modified electrode for highly sensitive flow based non-enzymatic glucose sensor, Sensors and Actuators B-Chemical, 246 (2017) 854-863.

[39] A. Kumar, R. Mishra, Y. Reinwald, S. Bhat, Cryogels: Freezing unveiled by thawing, Materials Today, 13 (2010) 42-44.

[40] H.S. Wroblowa, Y.C. Pan, G. Razumney, Electroreduction of oxygen - new mechanistic criterion, Journal of Electroanalytical Chemistry, 69 (1976) 195-201.

[41] I. Katsounaros, W.B. Schneider, J.C. Meier, U. Benedikt, P.U. Biedermann, A.A. Auer, K.J.J. Mayrhofer, Hydrogen peroxide electrochemistry on platinum: towards understanding the oxygen reduction reaction mechanism, Physical Chemistry Chemical Physics, 14 (2012) 7384-7391.

[42] R. Kerr, C. Pozo-Gonzalo, M. Forsyth, B. Winther-Jensen, Influence of the Polymerization Method on the Oxygen Reduction Reaction Pathway on PEDOT, ECS Electrochemistry Letters, 2 (2013) F29-F31.

[43] S.Y. Sawant, T.H. Han, M.H. Cho, Metal-Free Carbon-Based Materials: Promising Electrocatalysts for Oxygen Reduction Reaction in Microbial Fuel Cells, International Journal of Molecular Sciences, 18 (2017).

[44] Z. Zeng, T. Zhang, Y.Y. Liu, W.D. Zhang, Z.Y. Yin, Z.W. Ji, J.J. Wei, Magnetic Field-Enhanced 4-Electron Pathway for Well-Aligned Co3O4/Electrospun Carbon Nanofibers in the Oxygen Reduction Reaction, Chemsuschem, 11 (2018) 580-588.

[45] X.X. Huang, Y.Z. Wang, W. Li, Y.L. Hou, Noble metal-free catalysts for oxygen reduction reaction, Science China-Chemistry, 60 (2017) 1494-1507.

[46] C.S. Foote, J.S. Valentine, A. Greenberg, J.F. Liebman, Active oxygen in chemistry, Blackie Academic & Professional1995.

[47] R. Kerr, C. Pozo-Gonzalo, M. Forsyth, B. Winther-Jensen, The Reduction of Oxygen on Iron(II) Oxide/Poly(3,4-ethylenedioxythiophene) Composite Thin Film Electrodes, Electrochimica Acta, 154 (2015) 142-148.

[48] A.A. Karyakin, O.V. Gitelmacher, E.E. Karyakina, Prussian Blue based first-generation biosensor - a sensitive amperometric electrode for glucose, Analytical Chemistry, 67 (1995) 2419-2423.

[49] A.A. Karyakin, E.E. Karyakina, Prussian Blue-based 'artificial peroxidase' as a transducer for hydrogen peroxide detection. Application to biosensors, Sensors and Actuators B-Chemical, 57 (1999) 268-273.

[50] T.Y. Dai, X.J. Jiang, S.H. Hua, X.S. Wang, Y. Lu, Facile fabrication of conducting polymer hydrogels via supramolecular self-assembly, Chemical Communications, (2008) 4279-4281.

[51] Z.Y. Yang, X.H. Zheng, J.B. Zheng, Facile Synthesis of Prussian Blue/Hollow Polypyrrole Nanocomposites for Enhanced Hydrogen Peroxide Sensing, Industrial & Engineering Chemistry Research, 55 (2016) 12161-12166.

[52] P.K. Lee, P.M. Nia, P.M. Woi, Facile self-assembled Prussian blue-polypyrrole nanocomposites on glassy carbon: Comparative synthesis methods and its electrocatalytic reduction towards H2O2, Electrochimica Acta, 246 (2017) 841-852.

[53] D. Alemu, H.Y. Wei, K.C. Ho, C.W. Chu, Highly conductive PEDOT:PSS electrode by simple film treatment with methanol for ITO-free polymer solar cells, Energy & Environmental Science, 5 (2012) 9662-9671.

[54] C. Karuwan, C. Sriprachuabwong, A. Wisitsoraat, D. Phokharatkul, P. Sritongkham, A. Tuantranont, Inkjet-printed graphene-poly(3,4-ethylenedioxythiophene):poly(styrene-sulfonate) modified on screen printed carbon electrode for electrochemical sensing of salbutamol, Sensors and Actuators B-Chemical, 161 (2012) 549-555.

[55] A.V. Volkov, K. Wijeratne, E. Mitraka, U. Ail, D. Zhao, K. Tybrandt, J.W. Andreasen, M. Berggren, X. Crispin, I.V. Zozoulenko, Understanding the Capacitance of PEDOT:PSS, Advanced Functional Materials, 27 (2017).

[56] H.S. Park, S.J. Ko, J.S. Park, J.Y. Kim, H.K. Song, Redox-active charge carriers of conducting polymers as a tuner of conductivity and its potential window, Scientific Reports, 3 (2013).

[57] S. Chao, M.S. Wrighton, Solid-state microelectrochemistry - electrical characteristics of a solid-state microelectrochemical transistor based on poly(3methylthiophene), Journal of the American Chemical Society, 109 (1987) 2197-2199.

[58] G.P. Kittlesen, H.S. White, M.S. Wrighton, Chemical derivatization of microelectrode arrays by oxidation of pyrrole and N-methylpyrrole. Fabrication of molecule-based electronic devices, Journal of the American Chemical Society, 106 (1984) 7389-7396.

[59] Z. Algharaibeh, P.G. Pickup, Charge trapping in poly(1-amino-anthraquinone) films, Electrochimica Acta, 93 (2013) 87-92.

[60] B.D. Paulsen, K. Tybrandt, E. Stavrinidou, J. Rivnay, Organic mixed ionic–electronic conductors, Nature Materials, (2019).

[61] J. Rivnay, S. Inal, B.A. Collins, M. Sessolo, E. Stavrinidou, X. Strakosas, C. Tassone, D.M. Delongchamp, G.G. Malliaras, Structural control of mixed ionic and electronic transport in conducting polymers, Nature Communications, 7 (2016).

[62] Y.Y. Liu, H.T. Wang, D.C. Lin, J. Zhao, C. Liu, J. Xie, Y. Cui, A Prussian blue route to nitrogen-doped graphene aerogels as efficient electrocatalysts for oxygen reduction with enhanced active site accessibility, Nano Research, 10 (2017) 1213-1222.

[63] R.F. Zhou, Y. Zheng, M. Jaroniec, S.Z. Qiao, Determination of the Electron Transfer Number for the Oxygen Reduction Reaction: From Theory to Experiment, Acs Catalysis, 6 (2016) 4720-4728.

[64] A. Damjanovic, M.A. Genshaw, J.O.M. Bokris, Distinction between Intermediates Produced in Main and Side Electrodic Reactions, Journal of Physical Chemistry, 43 (1966) 4057–4059.

[65] N.S. Georgescu, A.J.J. Jebaraj, D. Scherson, A Critical Assessment of X-H2O2 as a Figure of Merit for Oxygen Reduction Electrocatalysts in Aqueous Electrolytes, ECS Electrochemistry Letters, 4 (2015) P39-P42.